Metallization of Shock-Compressed Liquid Ammonia

A. Ravasio,[1,*] M. Bethkenhagen,[2,3] J.-A. Hernandez,[1,4] A. Benuzzi-Mounaix,[1] F. Datchi,[5] M. French,[3] M. Guarguaglini,[1] F. Lefevre,[1] S. Ninet,[5] R. Redmer,[3] and T. Vinci[1]

[1]*LULI, CNRS, CEA, École Polytechnique—Institut Polytechnique de Paris, route de Saclay, 91128 Palaiseau cedex, France*

[2]*École Normale Supérieure de Lyon, Université Lyon 1, Laboratoire de Géologie de Lyon, CNRS UMR 5276, 69364 Lyon Cedex 07, France*

[3]*Institut für Physik, Universität Rostock, 18051 Rostock, Germany*

[4]*Centre for Earth Evolution and Dynamics, University of Oslo, N-0315 Oslo, Norway*

[5]*Institut de Minéralogie, de Physique des Matériaux et de Cosmochimie (IMPMC), Sorbonne Université, CNRS UMR 7590, MNHN, 4 place Jussieu, F-75005 Paris, France*

(Received 18 August 2020; revised 5 November 2020; accepted 10 December 2020; published 13 January 2021)

Ammonia is predicted to be one of the major components in the depths of the ice giant planets Uranus and Neptune. Their dynamics, evolution, and interior structure are insufficiently understood and models rely imperatively on data for equation of state and transport properties. Despite its great significance, the experimentally accessed region of the ammonia phase diagram today is still very limited in pressure and temperature. Here we push the probed regime to unprecedented conditions, up to ∼350 GPa and ∼40 000 K. Along the Hugoniot, the temperature measured as a function of pressure shows a subtle change in slope at ∼7000 K and ∼90 GPa, in agreement with *ab initio* simulations we have performed. This feature coincides with the gradual transition from a molecular liquid to a plasma state. Additionally, we performed reflectivity measurements, providing the first experimental evidence of electronic conduction in high-pressure ammonia. Shock reflectance continuously rises with pressure above 50 GPa and reaches saturation values above 120 GPa. Corresponding electrical conductivity values are up to 1 order of magnitude higher than in water in the 100 GPa regime, with possible significant contributions of the predicted ammonia-rich layers to the generation of magnetic dynamos in ice giant interiors.

DOI: 10.1103/PhysRevLett.126.025003

As an archetypal hydrogen-bonded system, the properties of ammonia (NH_3) at high pressures (P) and temperatures (T) are of particular interest in solid state physics and chemistry [1–3]. For temperatures up to 10 000 K and pressures up to 500 GPa, theoretical studies predict an exceptionally rich phase diagram, including fluid phases of different chemical composition, solid, and superionic phases [4–6]. Unveiling these extremely intriguing behaviors has also crucial impact on planetary science because NH_3 has a significant cosmic abundance. As a part of the so-called "planetary ice" (mixtures of water, ammonia, and methane), it is believed to be found in a wide range of thermodynamic conditions in planets and their satellites [7–10], both within our Solar System and beyond [11–13]. Adiabatic interior models of Uranus and Neptune predict that planetary ice exists between 20 to 600 GPa and 2000 to 7000 K [7,14–18], which possibly coincides with the stability range for superionic ammonia. Recent models [19–21] more consistent with Uranus' low luminosity observations predict much warmer interiors, with temperatures up to 25 000 K, where ammonia would rather be a warm dense ionized fluid [4,6,22,23]. These nonadiabatic models highly rely on transport properties of the planetary ice at such high temperatures, which are mostly unavailable to date. Moreover, the discovery of hot Neptune exoplanets, like Gliese 436b, further extends the necessity of exploring a wide range of thermodynamic conditions [24]. Accurate determination of the high-pressure ammonia equation of state is hence required to build more reliable interior models accounting for planetary ice as a complex mixture [17,19,25] and overcoming the often used, yet too simplistic, approach that considers planetary ice as made of pure water. Similarly, the NH_3 transport properties, such as electrical conductivity, are crucial to address Uranus' and Neptune's peculiar magnetic fields [26–28].

Despite its importance, experimental studies of the high pressure behavior of ammonia remain very scarce and limited to a narrow thermodynamic range. Measurements in diamond anvil cells have characterized the equation of state and phase diagram up to 200 GPa at 300 K, but reached at most ∼40 GPa at higher temperatures (∼3000 K) [29–36]. Few studies have been carried out employing dynamic compression methods, mainly at gas-gun facilities, providing shock compression data up to 70 GPa [37–42]. However, no reflectivity data were obtained, only two temperature points were reported [40] and only two electrical conductivity data points exceeded 40 GPa [41]. The dearth in experimental data is undoubtedly linked to

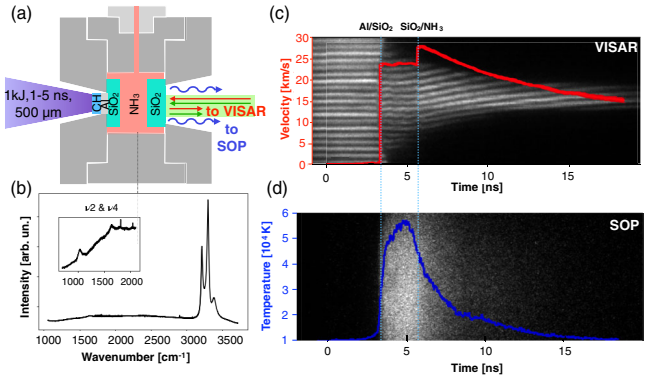

FIG. 1. (a) Schematic experimental setup of the laser pulse inducing shock compression in the liquid ammonia sample. (b) Raman spectrum of the sample indicative of pure liquid NH_3 with $\nu_1 - \nu_3$ stretching band around 3300 cm^{-1} as well as ν_2 and ν_4 modes (inset) at 1200 and 1600 cm^{-1}, respectively. (c) VISAR signal and (d) SOP data together with the extracted velocity and temperature measurements. For this shot, laser energy and pulse length were, respectively, 816 J and 2 ns.

the severe difficulties in preparing appropriate samples for high pressure experiments, in particular those using laser-driven shocks.

In this work, we report on the first laser-generated shock compression experiment in ammonia, which allowed us to study the equation of state and optical reflectivity (tightly linked to electronic conductivity) in an unprecedented regime, up to ~350 GPa and 40 000 K, together with new *ab initio* calculations.

The experiment was performed at the LULI2000 laser facility at the LULI Laboratory in France. The setup is shown schematically in Fig. 1(a). A long pulse ($\tau_L \sim 1.5 - 5$ ns) high-energy (E_L up to 1 kJ at $\lambda_L =$ 527 nm) laser beam was focused (~500 μm smoothed focal spot) on the target to generate a compression shock wave. In order to reach relevant pressures, we have conceived and assembled a specific target capable of accommodating liquid ammonia and compatible with standard laser-shock experiments. Gaseous NH_3 was first condensed at low temperatures (~243 K) in a small stainless steel cell target. Two thin α-quartz windows of 50 and 250 μm were used at the front (laser-side) and back (diagnostic side) of the cell, respectively, to ensure tightness and allow optical probing. A CH-Al pusher was glued on the outer part of the front side SiO_2 window to avoid any contamination of the sample. The system was then brought to ambient temperature, allowing an outgoing controlled flow to maintain an almost constant pressure and avoid breaking of the thin quartz windows under the thermal pressure increase. Finally, the initial Hugoniot state was fixed at 14 bar, room temperature (~295 K), and a density of 0.61 g/cm^3 (based on NIST database). The Raman spectrum of the filled cell is consistent with that of pure liquid ammonia without any measurable impurities [see Fig. 1(b)]. Visible diagnostics were used to probe shocked ammonia. A dual-channel velocity interferometer system for any reflector (VISAR) [43,44] operated at 532 nm and 1064 nm (sensitivities of 4.96 and 12.81 km/s) was used to measure the time-dependent shock velocity for equation of state measurements and reflectivity. The shock-front reflectivity at 532 nm was also measured independently with a reflectometer. A streaked optical pyrometer (SOP) [45–47] collected the self-emission of the shocked sample as a function of time to gather temperature estimation. Typical experimental data are shown in Figs. 1(c) and 1(d). Quartz (front side window) and ammonia are both rapidly ionized and transformed into a reflecting state upon shock compression. The instantaneous shock velocity in both materials could therefore be measured with the VISARs, knowing the values of the quartz and ammonia pristine refractive indices (n_0^{Qz} and $n_0^{NH_3}$, respectively) (see Supplemental Material [51]). Using quartz as *in situ* standard and applying impedance mismatch [48,49] together with the Rankine-Hugoniot relations [50] we get the thermodynamic conditions (mass density ϱ, pressure P, and internal energy E) in shocked ammonia at the SiO_2/NH_3 interface [51].

In addition to the experiment, we performed *ab initio* simulations using density functional theory molecular dynamics (DFT-MD) using VASP [67–70]. The Hugoniot states were calculated based on previous *ab initio* EOS data [6] derived with the Perdew-Burke-Ernzerhof (PBE) exchange-correlation functional [71]. Here, we extended these calculations and calculated reflectivity and dc electrical conductivity with both the PBE and the HSE [72,73] hybrid functional [51].

The experimental data for the Hugoniot are presented in Fig. 2. A total of 20 Hugoniot data points were recorded over the range 35–350 GPa, represented as dot symbols in Fig. 2. Also shown are previous experimental results from gas-gun facilities (starting densities $\varrho_0 = 0.69$ g/cm^3) and the Hugoniots from *ab initio* calculations performed in this work ($\varrho_0 = 0.61$ and $\varrho_0 = 0.69$ g/cm^3) and in Li *et al.* [22] ($\varrho_0 = 0.60$ and $\varrho_0 = 0.69$ g/cm^3). For low pressures, the Hugoniot curves are rather insensitive to the slightly different initial densities and our data are consistent with the gas gun data. Moreover, our experimental dataset is consistent with our theoretical predictions over the whole probed region. Because of the large impedance mismatch and the consistent thickness of the target, the shock wave is not sustained during its propagation in the ammonia sample. Following the decay of the compression wave as it traveled through the sample, we also obtained continuous time measurements of the temperature and reflectivity as a function of shock velocity (or of pressure, density and internal energy, after applying the corresponding relation from the Hugoniot data).

Temperature is one of the most difficult parameters to access and up to now only two experimental data points

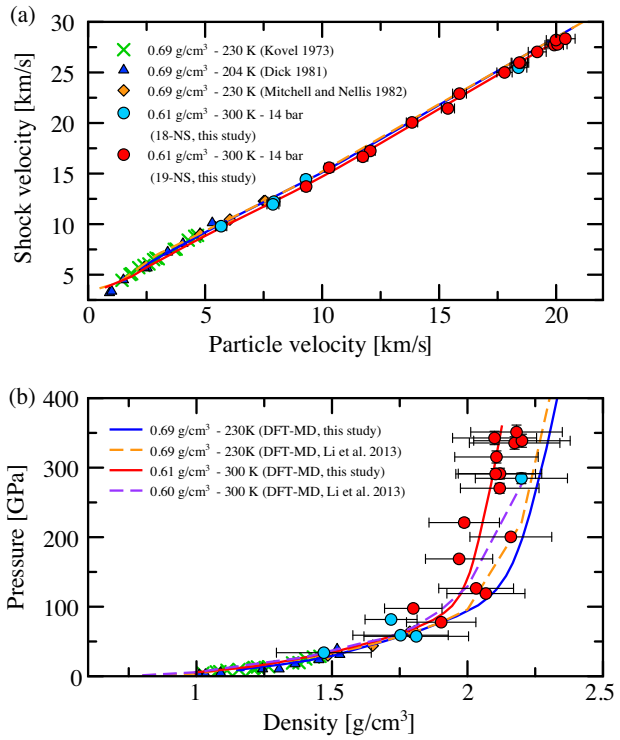

FIG. 2. Hydrodynamic conditions probed in shocked liquid ammonia ($\varrho_0 = 0.61$ g/cm^3). (a) Relation between shock and particle velocities. Also shown are previous measurements at an initial density of 0.69 g/cm^3 [37,38,74] and the previous (dashed lines) and present (continuous lines) DFT-MD data considering both initial states. (b) Corresponding pressure-density diagram.

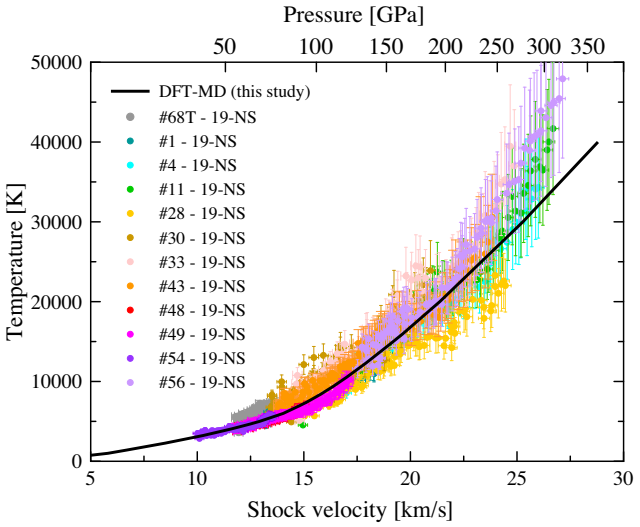

FIG. 3. Experimental (circles) and theoretical (black line) temperature of shocked ammonia as a function of the shock velocity along the 0.61 g/ cm^3 Hugoniot. Each circle represents a time-resolved measurement during the propagation of a decaying shock with typical error bars. The pressure scale on the top x axis is obtained by applying the $U_s - U_p$ linear relation derived from experimental measurements.

were available at ~4000 K [40]. Our dataset, shown in Fig. 3, provides a much wider ensemble up to very high temperatures. The consistency with calculations is remarkable, except for the highest points where the experimental uncertainties are larger. In particular, in both calculations and experiment we find that the shock temperature increases continuously up to ~7000 K (~90 GPa), where a slight change of slope occurs, see Fig. 3. In solids this kind of behavior is often linked to phase transitions, including melting (Refs. [75,76]). To understand the origin of this feature in ammonia, we have computed the ion-ion pair correlation functions along the Hugoniot, shown in Fig. 4. The analysis of these calculations indicates that the observed change in slope in the $P - T$ curve is caused by dissociation processes in the molecular liquid and its transformation into a plasma state. In the N-H pair correlation function in Fig. 4(b), the drop of the intramolecular bond peak at 1.08 Å with increasing temperature illustrates the gradual dissociation of the ammonia molecules. We also observe additional peaks in the H-H and N-N pair correlation functions above 2000 K, which are indicative of the formation of H_2 and N_2 molecules. Even more complex and very short-lived molecules such as N_2H_4 and HN_3 were observed from visual inspections of the ionic trajectories in the DFT-MD. It can be seen that the characteristic H_2 signal in Fig. 4(a) vanishes above 5000 K and that the broad feature corresponding to different forms of N-N bonding [between 1.0 and 1.5 Å in Fig. 4(c)] reaches its maximum at 7000–8000 K. This implies that the molecular NH_3 liquid transforms through continuous dissociation and ionization processes into a plasma. Additionally, diffusion coefficients and vibrational spectra confirm that NH_3 molecules dissociate between 6000 and 8000 K (see Supplemental Material [51]). This behavior reveals that along the Hugoniot the chemistry in ammonia is richer in small molecular species compared to water, which dissociates into simple ionic and atomic species at similar shock pressures [77].

Figure 5(a) shows the measured reflectivities at 532 and 1064 nm, together with the DFT-MD calculated values, using either the PBE [71] or HSE [72,73] exchange-correlation functionals. Included are also predictions from Ref. [22]. Our data suggest a gradual rise in shock reflectivity with pressure, with a smooth transition from a low- to a highly reflecting state between ~50 and ~120 GPa.

Present calculations are in good agreement with the experimental data. In particular, they match the saturation values at both wavelengths remarkably well. We find a relatively small influence of the exchange-correlation functional, due to partial compensation of errors that occurs in the Fresnel formula between the indexes of refraction for the initial (n_0) and final (n) Hugoniot states (see the Supplemental Material [51]). Note that the HSE calculations reproduce the initial index of refraction ($n_0^{\mathrm{HSE}} = 1.34$)

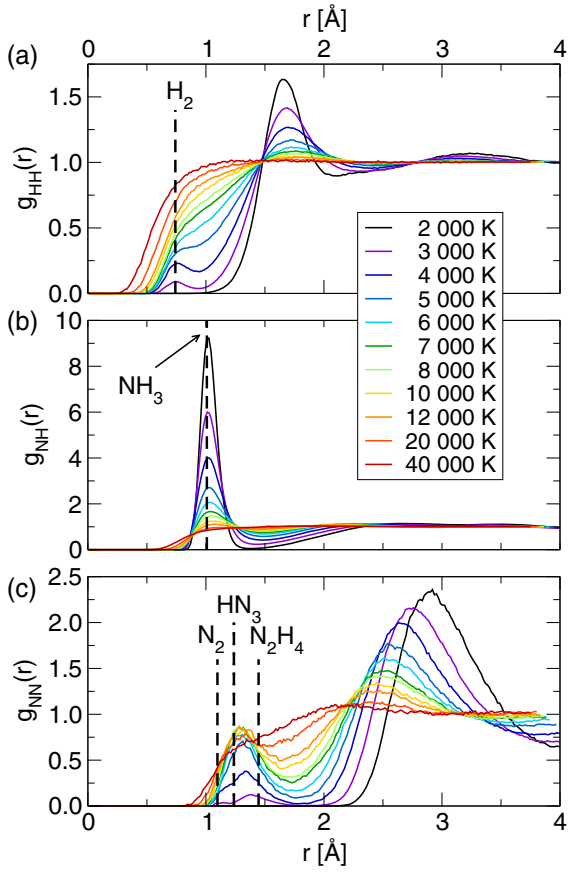

FIG. 4. (a) H-H, (b) N-H, and (c) N-N pair correlation functions for different temperatures along the Hugoniot (solid lines). The dashed lines indicate bond lengths in various molecules that were visually observed in the simulations.

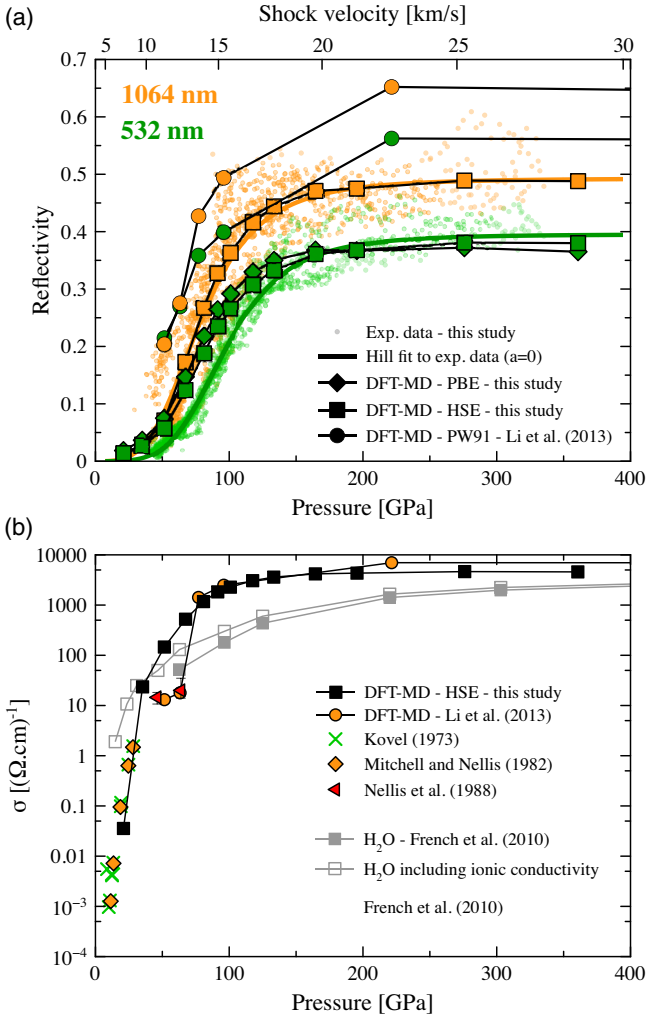

FIG. 5. (a) Reflectivity at 532 (green) and 1064 nm (orange) versus pressure. Small orange and green dots correspond to time-resolved experimental reflectivities measured in 11 decaying shots. Thick orange and green lines are Hill fits to the experimental data with the reflectivity imposed to be zero at $U_s = 0$ km/s. Diamonds and squares correspond to the DFT reflectivities computed in this study, respectively, with the PBE and HSE functionals. Large dots show DFT reflectivities from Ref. [22]. (b) Calculated dc electrical conductivity of NH_3 along the Hugoniot (black squares) compared to previous DFT-MD results [22] and experimental data [38,41,74]. The electronic and total electrical conductivity along the principal H_2O Hugoniot are also shown as gray solid and open squares, respectively [77].

much better than the PBE calculations ($n_0^{\mathrm{PBE}} = 1.42$) if compared to the experimental value ($n_0^{\mathrm{exp}} = 1.32$). The disagreement between our DFT-MD results and previous calculations is mainly explained by an incorrect setting of $n_0 = 1$ by Li *et al.* [22], which leads to a shifted onset of reflectivity increase and significantly too high saturation values in their data.

Reflectivity is closely related to dc electrical conductivity $\sigma(\omega = 0)$, which is a crucial quantity for, e.g., plasma diagnostics and planetary dynamo models. Our *ab initio* calculations show that the frequency behavior of $\sigma(\omega)$ is very different from a Drude behavior (see Supplemental Material [51]), which is often assumed to derive dc conductivities from optical reflectivities [78–81]. The calculated dc electronic conductivity is regarded as highly reliable considering the excellent agreement between *ab initio* and experimental reflectivity data. It rises systematically with Hugoniot pressure [Fig. 5(b)]. The lowest dc conductivity point at ~21 GPa and 2000 K is in good agreement with previous experiments [38,74]. Interestingly, we find significantly higher values than those measured in Ref. [41] between 50 and 75 GPa and calculated in Li *et al.* [22]. A possible explanation for this deviation may be the higher initial density of $\varrho = 0.69$ g/cm^3 compared to our Hugoniot, so that results from Refs. [22,41] between 50 and 75 GPa might describe a different phase, most likely the superionic phase [6]. Above 75 GPa, the values calculated by Li *et al.* [22] agree reasonably well with our results. We also note that overall the NH_3 conductivity is larger than the one of water along the Hugoniot. Even when the ionic contribution is added for water [77], the ammonia conductivity remains 1 order of magnitude higher in the

100 GPa regime, due to the different dissociation mechanisms, as discussed above.

In conclusion, we report novel equation of state measurements of warm dense ammonia in a previously unachieved regime, together with the first experimental evidence of ammonia metallization we observed in the reflectivity. These high quality data on such an experimentally challenging compound provide a unique benchmark for our *ab initio* calculations. The simulations indicate a complex dissociation mechanism in ammonia, comprising three regimes: a molecular fluid, where NH_3 molecules still persist, a complex fluid above 20 GPa, in which NH_3 molecules start to dissociate and N_2 and N_3 bounded molecules are formed, and a completely dissociated plasma state above 90 GPa. The electrical conductivity is surprisingly high and *one* order of magnitude higher than that of water at ∼100 GPa. This finding is particularly useful to revisit dynamo models of Uranus and Neptune magnetic fields, as the only existing conductivity data at lower pressures suggest the opposite trend [39]. Models that entirely disregarded ammonia in the past should now consider the possible contribution of the predicted ammonia-rich layers [82] to have better insights of the dynamo process in ice giant planets. Future work should extend our study to the superionic domain to estimate the extent and the physical properties of the potential superionic layers within ice giant planets.

The authors acknowledge the crucial contribution of the LULI2000 laser and support teams to the success of the experiments. The authors also would like to thank D. Tondelier (LPICM), C. Kaimakian, and C. Gosmini for technical support, as well as N. Ozaki for useful discussions. This research was supported by the French National Research Agency (ANR) through the projects POMPEI (Grant No. ANR-16-CE31-0008) and SUPER-ICES (Grant No. ANR-15-CE30-008-01). M. B., M. F., and R. R. gratefully acknowledge support by the by the Deutsche Forschungsgemeinschaft (DFG) within the Research Unit FOR 2440. M. B. was additionally supported by the European Union within the Marie Skłodowska-Curie actions (xICE grant 894725). The DFT-MD calculations were performed at the North-German Supercomputing Alliance (HLRN) facilities. J.-A.H. acknowledges support from the Research Council of Norway through its Centres of Excellence funding scheme, project No. 223272. The Raman measurements used the spectroscopy platform of IMPMC with the assistance of K. Beneut.

*alessandra.ravasio@polytechnique.fr

[1] Y. Liu and M. E. Tuckerman, J. Phys. Chem. B **105**, 6598 (2001).
[2] A. D. Fortes, J. P. Brodholt, I. G. Wood, and L. Voadlo, J. Chem. Phys. **118**, 5987 (2003).
[3] A. Hermann, in *Reviews in Computational Chemistry*, edited by A. L. Parrill and K. B. Lipkowitz (Wiley, New York, 2017), https://doi.org/10.1002/9781119356059.ch1.
[4] C. Cavazzoni, G. L. Chiarotti, S. Scandolo, E. Tosatti, M. Bernasconi, and M. Parrinello, Science **283**, 44 (1999).
[5] C. J. Pickard and R. J. Needs, Nat. Mater. **7**, 775 (2008).
[6] M. Bethkenhagen, M. French, and R. Redmer, J. Chem. Phys. **138**, 234504 (2013).
[7] W. B. Hubbard and J. J. MacFarlane, J. Geophys. Res. **85**, 225 (1980).
[8] W. B. Hubbard, W. J. Nellis, A. C. Mitchell, N. C. Holmes, S. S. Limaye, and P. C. McCandless, Science **253**, 648 (1991).
[9] B. Journaux, K. Kalousova, C. Sotin, G. Tobie, S. Vance, J. Saur, O. Bollengier, L. Noack, T. Ruckriemen-Bez, T. Van Hoolst, K. M. Soderlund, and J. M. Brown, Space Sci. Rev. **216**, 7 (2020).
[10] R. Helled, N. Nettelmann, and T. Guillot, Space Sci. Rev. **216**, 38 (2020).
[11] W. J. Borucki *et al.*, Astrophys. J. **736**, 19 (2011).
[12] F. Fressin, G. Torres, D. Charbonneau, S. T. Bryson, J. Christiansen, C. D. Dressing, J. M. Jenkins, L. M. Walkowicz, and N. M. Batalha, Astrophys. J. **766**, 81 (2013).
[13] L. Zeng, S. B. Jacobsen, D. D. Sasselov, M. I. Petaev, A. Vanderburg, M. Lopez-Morales, J. Perez-Mercader, T. R. Mattsson, G. Li, M. Z. Heising, A. S. Bonomo, M. Damasso, T. A. Berger, H. Cao, A. Levi, and R. D. Wordsworth, Proc. Natl. Acad. Sci. U.S.A. **116**, 9723 (2019).
[14] R. Redmer, T. R. Mattsson, N. Nettelmann, and M. French, Icarus **211**, 798 (2011).
[15] R. Helled, J. Anderson, M. Podolak, and G. Schubert, Astrophys. J. **726**, A15 (2011).
[16] N. Nettelmann, R. Helled, J. Fortney, and R. Redmer, Planet. Space Sci. **77**, 143 (2013).
[17] M. Bethkenhagen, E. R. Meyer, S. Hamel, N. Nettelmann, M. French, L. Scheibe, C. Ticknor, L. A. Collins, J. D. Kress, J. J. Fortney, and R. Redmer, Astrophys. J. **848**, 67 (2017).
[18] L. Scheibe, N. Nettelmann, and R. Redmer, Astron. Astrophys. **632**, A70 (2019).
[19] N. Nettelmann, K. Wang, J. Fortney, S. Hamel, S. Yellamilli, M. Bethkenhagen, and R. Redmer, Icarus **275**, 107 (2016).
[20] M. Podolak, R. Helled, and G. Schubert, Mon. Not. R. Astron. Soc. **487**, 2653 (2019).
[21] A. Vazan and R. Helled, Astron. Astrophys. **633**, A50 (2020).
[22] D. F. Li, P. Zhang, and J. Yan, J. Chem. Phys. **139**, 134505 (2013).
[23] D. F. Li, C. Wang, J. Yan, Z. G. Fu, and P. Zhang, Sci. Rep. **7**, 12338 (2017).
[24] N. Nettelmann, U. Kramm, R. Redmer, and Neuhäuser, Astron. Astrophys. **523**, A26 (2010).
[25] M. Guarguaglini, J. A. Hernandez, T. Okuchi, P. Barroso, A. Benuzzi-Mounaix, M. Bethkenhagen, R. Bolis, E. Brambrink, M. French, Y. Fujimoto, R. Kodama, M. Koenig, F. Lefevre, K. Miyanishi, N. Ozaki, R. Redmer, T. Sano, Y. Umeda, T. Vinci, and A. Ravasio, Sci. Rep. **9**, 10155 (2019).
[26] D. J. Stevenson, Space Sci. Rev. **152**, 651 (2010).
[27] S. Stanley and J. Bloxham, Icarus **184**, 556 (2006).
[28] K. M. Soderlund, M. H. Heimpel, E. M. King, and J. M. Aurnou, Icarus **224**, 97 (2013).

[29] S. Ninet and F. Datchi, J. Chem. Phys. **128**, 154508 (2008).
[30] F. Li, M. Li, Q. Cui, T. Cui, Z. He, Q. Zhou, and G. Zou, J. Chem. Phys. **131**, 134502 (2009).
[31] S. Ninet, F. Datchi, and A. M. Saitta, Phys. Rev. Lett. **108**, 165702 (2012).
[32] S. Ninet, F. Datchi, P. Dumas, M. Mezouar, G. Garbarino, A. Mafety, C. J. Pickard, R. J. Needs, and A. M. Saitta, Phys. Rev. B **89**, 174103 (2014).
[33] J. A. Queyroux, S. Ninet, G. Weck, G. Garbarino, T. Plisson, M. Mezouar, and F. Datchi, Phys. Rev. B **99**, 134107 (2019).
[34] J. A. Queyroux, S. Ninet, G. Weck, G. Garbarino, M. Mezouar, and F. Datchi, Phys. Rev. B **100**, 224104 (2019).
[35] J. G. O. Ojwang, R. S. McWilliams, X. Ke, and A. F. Goncharov, J. Chem. Phys. **137**, 064507 (2012).
[36] T. Palasyuk, I. Troyan, M. Eremets, V. Drozd, S. Medvedev, P. Zaleski-Ejgierd, E. Magos-Palasyuk, H. B. Wang, S. A. Bonev, D. Dudenko, and P. Naumov, Nat. Commun. **5**, 3460 (2014).
[37] R. D. Dick, J. Chem. Phys. **74**, 4053 (1981).
[38] A. C. Mitchell and W. J. Nellis, J. Chem. Phys. **76**, 6273 (1982).
[39] W. J. Nellis, D. C. Hamilton, N. C. Holmes, H. B. Radousky, F. H. Ree, A. C. Mitchell, and M. Nicol, Science **240**, 779 (1988).
[40] H. B. Radousky, A. C. Mitchell, and W. J. Nellis, J. Chem. Phys. **93**, 8235 (1990).
[41] W. J. Nellis, N. C. Holmes, A. C. Mitchell, D. C. Hamilton, and M. Nicol, J. Chem. Phys. **107**, 9096 (1997).
[42] D. M. Dattelbaum, J. M. Lang, P. M. Goodwin, L. L. Gibson, W. P. Gammel, J. D. Coe, C. Ticknor, and J. A. Leiding, J. Chem. Phys. **150**, 024305 (2019).
[43] L. M. Barker and R. E. Hollenbach, J. Appl. Phys. **43**, 4669 (1972).
[44] P. M. Celliers, D. K. Bradley, G. W. Collins, D. G. Hicks, T. R. Boehly, and W. J. Armstrong, Rev. Sci. Instrum. **75**, 4916 (2004).
[45] N. C. Holmes, Rev. Sci. Instrum. **66**, 2615 (1995).
[46] T. A. Hall, A. Benuzzi, D. Batani, D. Beretta, S. Bossi, B. Faral, M. Koenig, J. Krishnan, T. Löwer, and M. Mahdieh, Phys. Rev. E **55**, R6356 (1997).
[47] J. E. Miller, T. R. Boehly, A. Melchior, D. D. Meyerhofer, P. M. Celliers, J. H. Eggert, D. G. Hicks, C. M. Sorce, J. A. Oertel, and P. M. Emmel, Rev. Sci. Instrum. **78**, 034903 (2007).
[48] J. W. Forbes, *Shock Wave Compression of Condensed Matter* (Springer, New York, 2012).
[49] S. Brygoo, M. Millot, P. Loubeyre, A. E. Lazicki, S. Hamel, T. Qi, P. M. Celliers, F. Coppari, J. H. Eggert, D. E. Fratanduono *et al.*, J. Appl. Phys. **118**, 195901 (2015).
[50] Y. B. Zel'dovich and Y. P. Raizer, in *Physics of Shock Waves and High-Temperature Hydrodynamic Phenomena* (Dover Publications, New York, 2002), pp. XXVII, 916 S.
[51] See Supplemental Material at http://link.aps.org/supplemental/10.1103/PhysRevLett.126.025003 for further experimental details, which includes Refs. [52–59] and for further computational details, which includes Refs. [60–67].
[52] G. Ghosh, Opt. Commun. **163**, 95 (1999).
[53] M. Gauthier, P. Pruzan, J. C. Chervin, and A. Polian, Solid State Commun. **68**, 149 (1988).
[54] T. Kume, M. Daimon, S. Sasaki, and H. Shimizu, Phys. Rev. B **57**, 13347 (1998).
[55] C. W. Robertson and D. Williams, J. Opt. Soc. Am. **63**, 188 (1973).
[56] R. Tillner-Roth, F. Harms-Watzenberg, and H. Baehr, DKV Tagungsbericht **20**, 67 (1993).
[57] G. Huser, V. Recoules, N. Ozaki, T. Sano, Y. Sakawa, G. Salin, B. Albertazzi, K. Miyanishi, and R. Kodama, Phys. Rev. E **92**, 063108 (2015).
[58] T. Qi, M. Millot, R. G. Kraus, S. Root, and S. Hamel, Phys. Plasmas **22**, 062706 (2015).
[59] M. Gregor, R. Boni, A. Sorce, J. Kendrick, C. McCoy, D. Polsin, T. Boehly, P. Celliers, G. Collins, D. Fratanduono *et al.*, Rev. Sci. Instrum. **87**, 114903 (2016).
[60] S. Nosé, J. Chem. Phys. **81**, 511 (1984).
[61] A. Baldereschi, Phys. Rev. B **7**, 5212 (1973).
[62] R. Kubo, J. Phys. Soc. Jpn. **12**, 570 (1957).
[63] D. A. Greenwood, Proc. Phys. Soc. London **71**, 585 (1958).
[64] B. Holst, M. French, and R. Redmer, Phys. Rev. B **83**, 235120 (2011).
[65] M. Gajdoš, K. Hummer, G. Kresse, J. Furthmüller, and F. Bechstedt, Phys. Rev. B **73**, 045112 (2006).
[66] P. H. Berens, D. H. J. Mackay, G. M. White, and K. R. Wilson, J. Chem. Phys. **79**, 2375 (1983).
[67] G. Kresse and J. Hafner, Phys. Rev. B **47**, 558 (1993).
[68] G. Kresse and J. Hafner, Phys. Rev. B **48**, 13115 (1993).
[69] G. Kresse and J. Hafner, Phys. Rev. B **49**, 14251 (1994).
[70] G. Kresse and J. Furthmüller, Phys. Rev. B **54**, 11169 (1996).
[71] J. P. Perdew, K. Burke, and M. Ernzerhof, Phys. Rev. Lett. **77**, 3865 (1996).
[72] J. Heyd, G. E. Scuseria, and M. Ernzerhof, J. Chem. Phys. **118**, 8207 (2003).
[73] J. Heyd, G. E. Scuseria, and M. Ernzerhof, J. Chem. Phys. **124**, 219906 (2006).
[74] M. I. Kovel, The shock wave Hugoniot and electrical conductivity of liquid ammonia in the pressure range 45 Kb to 282 Kb, Ph.D. Thesis, University of California, 1973.
[75] M. Millot, N. Dubrovinskaia, A. Černok, S. Blaha, L. Dubrovinsky, D. G. Braun, P. M. Celliers, G. W. Collins, J. H. Eggert, and R. Jeanloz, Science **347**, 418 (2015).
[76] R. S. McWilliams, D. K. Spaulding, J. H. Eggert, P. M. Celliers, D. G. Hicks, R. F. Smith, G. W. Collins, and R. Jeanloz, Science **338**, 1330 (2012).
[77] M. French, T. R. Mattsson, and R. Redmer, Phys. Rev. B **82**, 174108 (2010).
[78] P. M. Celliers *et al.*, Phys. Plasmas **11**, L41 (2004).
[79] M. D. Knudson, M. P. Desjarlais, R. W. Lemke, T. R. Mattsson, M. French, N. Nettelmann, and R. Redmer, Phys. Rev. Lett. **108**, 091102 (2012).
[80] T. Kimura, N. Ozaki, T. Sano, T. Okuchi, T. Sano, K. Shimizu, K. Miyanishi, T. Terai, T. Kakeshita, Y. Sakawa, and R. Kodama, J. Chem. Phys. **142**, 164504 (2015).
[81] M. Millot, S. Hamel, J. R. Rygg, P. M. Celliers, G. W. Collins, F. Coppari, D. E. Fratanduono, R. Jeanloz, D. C. Swift, and J. H. Eggert, Nat. Phys. **14**, 297 (2018).
[82] V. Naden Robinson, Y. C. Wang, Y. M. Ma, and A. Hermann, Proc. Natl. Acad. Sci. U.S.A. **114**, 9003 (2017).